Effects of functionalised reduced graphene oxide on frictional and wear properties of epoxy resin

R. Shah[1], T. Datashvili[2,3], T. Cai[1], J. Wahrmund[2], B. Menard[2], K. P. Menard[2,4], W. Brostow*[2] and J. Perez[1]

The effects of octadecylamine functionalised reduced graphene oxide (FRGO) on the frictional and wear properties of diglycidyl ether of bisphenol A epoxy are studied using pin on disc tribometry. The nanocomposites are prepared by adding 0·1, 0·2, 0·5 and 1·0 wt-% of FRGO to the epoxy. The addition of FRGO increases by more than an order of magnitude the sliding distance during which the dynamic friction is ≤0·1. After this distance, the friction sharply increases to the range of 0·4–0·5. We explain the increase in sliding distance during which the friction is low by formation of a transfer film from the nanocomposite to the pin. The wear rates in the low and high friction regimes are $\sim 1{\cdot}5 \times 10^{-4}$ and $5{\cdot}5 \times 10^{-4}$ mm^3 N^{-1} m^{-1} respectively. The nanocomposites exhibit a 79% increase in Young's modulus with 0·5 wt-% of FRGO, and an increase in glass transition and thermal degradation temperatures.

Keywords: Graphene, Epoxy, Nanocomposite, Friction, Wear

Introduction

Graphene is a material with a two-dimensional honeycomb lattice with sp^2 bonded carbon atoms.[1–5] Graphene has high mechanical strength and high electrical and thermal conductivities, making it potentially useful in the fabrication of polymer nanocomposites with enhanced mechanical, tribological, thermal and electrical properties.[6–11] Earlier publications dealt with various carbon materials including carbon black, carbon nanofibres, exfoliated graphite and carbon nanotubes (CNTs) as fillers in polymers to improve these properties.[12–17] Carbon nanotubes have been shown to be particularly effective due to their high mechanical strength, and high electrical and thermal conductivities.[12,18,19] It has been reported that the addition of 2 wt-% CNTs in epoxies doubles the Young's modulus.[13] The addition of 0·1 wt-% CNTs increases the electrical conductivity from 10^{-9} to 10^{-2} Sm^{-1},[14] and 1 wt-% increases the thermal conductivity by 80%.[15] In addition, CNTs have been reported to increase the glass transition temperature T_g of epoxies.[20] Carbon nanotubes functionalised with maleic anhydride and amino groups increase T_g by 10 and 14°C respectively.[21] Carbon nanotubes modified with non-ionic surfactants increase T_g by 25°C.[17] The increase in T_g has been attributed to the nanoscale dimensions of CNTs that result in good dispersion and adhesion at the molecular level, altering the chain dynamics.[22,23] In contrast, macroscopic fillers such as carbon fibre and graphite do not significantly affect T_g.[24,25]

In comparison to CNTs, graphene is less expensive to produce and more miscible due to its large surface area.[18] It has been reported that the addition of 0·4 wt-% of amine functionalised graphene to epoxy increases the Young's modulus by 60%.[26] The addition of 4 wt-% of graphene and 2·5 wt-% of surface modified graphene to epoxy increases T_g by ~8 and ~14°C respectively.[23] The addition of 1 wt-% of functionalised graphene to poly(acrylonitrile) increases T_g by as much as 40°C.[22] Other studies on graphene–epoxy nanocomposites have reported the effects of graphene oxide (GO) on curing,[27] graphene platelets on fracture properties,[23] functionalised GO on hardness, electrical conductivity and thermal properties[28] and organosilane functionalised graphene on thermal degradation and tensile strength.[29] Tribological studies of graphene–polymer nanocomposites have shown that the wear rate of polytetrafluoroethylene is significantly reduced by the addition of 10 wt-% of thermally reduced graphene platelets.[30] The friction and wear rate of nylon are lowered by modified GO.[31]

Epoxy resin is used in various aerospace and automotive applications due to its mouldability and good mechanical and thermal properties.[27,32,33] It would be of interest to study the tribological properties graphene–epoxy nanocomposites with the goal of lowering friction

[1]Department of Physics, University of North Texas, Denton, TX 76203, USA
[2]Laboratory of Advanced Polymers & Optimized Materials, Department of Materials Science and Engineering and Department of Physics, University of North Texas, 3940 North Elm Street, Denton TX 76207, USA
[3]Braskem America Inc., 550 Technology Drive, Pittsburgh PA 15219, USA
[4]PerkinElmer Analytical Sciences, Shelton, CT 06484, USA

*Corresponding author, email konradb09@gmail.com

Received 6 October 2013; accepted 4 March 2014
DOI 10.1179/1433075X14Y.0000000220

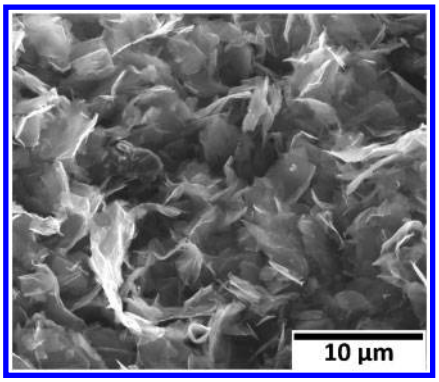

1 Scanning electron microscopy image of FRGO

and wear rates to extend their lifetime.[34–38] In this paper, we report the effects of octadecylamine (ODA) functionalised reduced GO (FRGO) on the friction and wear properties of diglycidyl ether of bisphenol A epoxy. The effects on the Young's modulus, T_g and thermal stability of the epoxy are also reported.

Experimental

Preparation of ODA FRGO

Graphene oxide was prepared using the Hummer method.[39] In brief, 5 g of graphite powder (325 mesh, Southwestern Graphite) and 2·5 g of $NaNO_3$ were added to 115 mL of concentrated H_2SO_4 at room temperature. The mixture was transferred to an ice bath, and 15 g of $KMnO_4$ was added under stirring conditions. The mixture was then transferred to a water bath to maintain the temperature within the range of 35–40°C. After half an hour, 235 mL of DI water was added to slow the reaction, and the mixture was stirred for 15 min. An additional 830 mL of water was added followed by the slow addition of H_2O_2 (30%). The mixture was then repeatedly filtered and washed with HCl (1 : 10) aqueous solution. The filtered material was dispersed in water using horn sonication, and centrifuged at 3500 rev min^{-1}. Residual acids and salt impurities were removed using dialysis for 10 days. Finally, the suspension was dried to a powder in an oven.

If the exfoliated GO were reduced at this stage, reaggregation of graphene layers would occur due to π–π interactions, which are difficult to undo using sonication.[40] Reaggregation can be significantly reduced by functionalising GO with ODA before reduction.[41] Octadecylamine functionalisation also facilitates the dispersion of FRGO in the polymer.[42,43] We carried out ODA functionalisation by dispersing 300 mg of GO powder in 300 mL of ethanol by sonication for 2 h, and then adding 450 mg of ODA in 45 mL of ethanol. The mixture was refluxed for 24 h at 90°C, and the solution was then repeatedly filtered and rinsed with ethanol to remove excess ODA. Octadecylamine functionalisation occurs by nucleophilic substitution reactions between the amine groups of ODA and the epoxide groups of GO.[44] Therefore, ODA functionalisation partially reduces GO; the presence of other oxygen containing functional groups such as hydroxyl and carbonyl groups remains. These groups can be reduced by reaction with hydrazine monohydrate without significant effects on ODA functionalisation.[45] For reduction, we dispersed functionalised GO powder in ethanol and hydrazine monohydrate. The mixture was refluxed at 90°C for 24 h, and the final product was repeatedly filtered and washed with ethanol, and then dried in a vacuum oven.

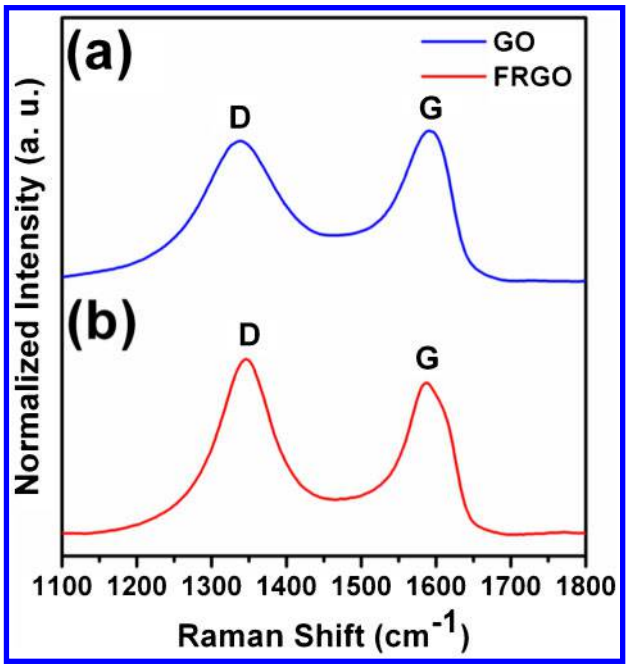

2 Raman spectra of *a* GO and *b* FRGO

Characterisation of FRGO

The surface morphology of FRGO powder was characterised using an FEI Nova 200 NanoLab scanning electron microscope (SEM), as shown in Fig. 1. We see that the lateral dimensions of the graphene flakes are a few micrometres. Micro-Raman spectroscopy was carried out using a Thermo Electron Almega XR spectrometer. Figure 2 shows Raman spectra of the GO and FRGO powders. The spectra are normalised so that the *G* peaks of the GO and FRGO have the same height. The *G* peak is due to first order scattering of E_{2g} phonons (in plane optical mode) of sp^2 hybridised carbon atoms close to the γ point.[45] As shown in Fig. 2*a*, the *G* peak in GO is at ~1593 cm^{-1}. The *G* peak is shifted from its value in graphite, of 1581 cm^{-1}, due to oxidation. Carbon materials also exhibit a *D* peak at ~1340 cm^{-1} due to defect induced zone boundary phonons.[46] The *D* peak in GO is due to a reduction in size of sp^2 hybridised domains due to oxidation.[45] The Raman spectrum of FRGO has *G* and *D* peaks at 1587 and 1346 cm^{-1} respectively, as shown in Fig. 2*b*. In FRGO, the *G* peak shifts towards the position of the *G* peak in graphite due to restoration of sp^2 hybridised domains.[47] The ratio of the intensities of the *D* and *G* peaks in FRGO is greater than that in GO due to a decrease in size of in plane sp^2 hybridised domains in FRGO due to reduction.[46] Our Raman results are in good agreement with previous reports on GO and FRGO.[48]

We further characterised the GO and FRGO using a VersaProbe X-ray photoelectron spectroscopy (XPS) system from Physical Electronics. The XPS spectra of GO and FRGO are shown in Fig. 3*a* and *b* respectively. The spectra for GO indicate covalently attached hydroxyl (C–OH), epoxide (–C–O–C–) and carboxylic (–O–C=O) oxygen groups at 286·5, 287·2 and 288·7 eV

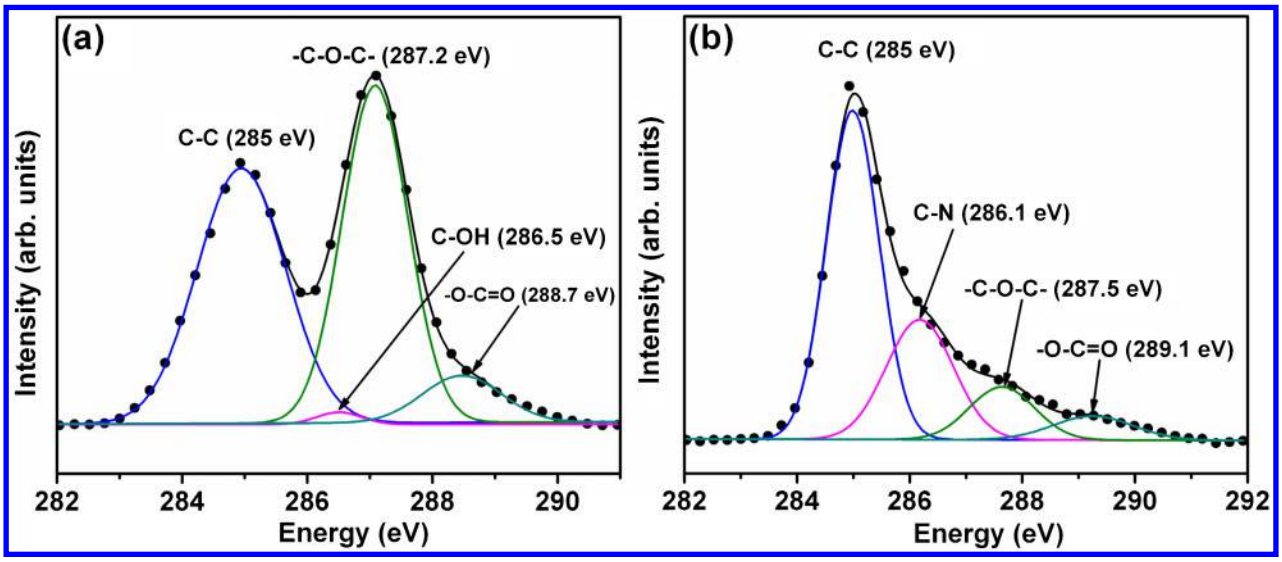

3 X-ray photoelectron spectroscopy spectra of *a* GO and *b* FRGO. Black circles represent raw data. Black line is fitted sum, and coloured lines are fitted peaks using software OMNIC for Almega 7

respectively, along with sp^2 hybridised C–C bonds at 285·0 eV. The XPS spectrum of FRGO shows that the intensity of oxygen containing functional groups is significantly reduced, and a new functional group appears at 286·1 eV, corresponding to C–N bonds that appear due to the functionalisation of GO with ODA. These results are also in good agreement with previous reports.[48]

Preparation of FRGO/epoxy nanocomposite

To synthesise the FRGO/epoxy nanocomposites, FRGO was dispersed in acetone (100 mg of FRGO in 100 mL of acetone) using sonication for 2 h in an ice bath. Varying amounts of epoxy resin (System Three Resin, Inc.) were then added, and the mixture was sonicated for 1 h. The acetone was evaporated by heating at 70°C. Residual acetone was removed by placing the mixture in a vacuum oven for 12 h at 70°C. After cooling to room temperature, a low viscosity slow curing agent (System Three Hardener Part B, no. 3) was added. The mixture was poured into silicone moulds of different shapes for various types of characterisation. The samples were cured for 24 h at room temperature.

Tensile testing

We have used an MTS system, applying a tensile rate of 10 mm min^{-1}, with a high load limit set-up at 5000 lbf. Testing was performed at room temperature of ~23°C.

Dynamic mechanical analysis

Dynamic mechanical analysis (DMA) was carried out using a PerkinElmer DMA8000 apparatus. The measurements were performed in single cantilever bending mode. Three frequencies were applied, namely, 0·1, 1·0 and 10·0 Hz. The differences between those sets of results were not significant; hence, results for 1·0 Hz are reported below. All deformations were 50 μm, so that strain was well <1%.

Thermal stability determination

The thermal stability of the nanocomposites was studied using a PerkinElmer TGA 7 thermogravimetric analyser (TGA). We have covered the range from 20 to 600°C at heating rate of 20°C min^{-1} under N_2 gas.

Tribological properties

We studied the frictional and wear properties of the nanocomposites using a Nanovea tribometer from Micro Photonics, Inc. A tungsten carbide ball with a diameter of 6 mm was used as the counter surface. All measurements were performed in air using 15 N normal load, 80 rev min^{-1} rotational speed and a circular track having a radius of 2 mm. Further details are provided near Fig. 7.

Tensile testing results

Figure 4 shows that the Young's modulus increases with the addition of FRGO for concentrations from 0·1 to 0·5 wt-%. The Young's modulus, tensile strength and strain at break for the various FRGO concentrations are shown in Table 1. For 0·5 wt-% FRGO, the Young's modulus increases by 75% from 1·23 to 2·15 GPa, while the tensile strength increases by 68%. Similar increases in the Young's modulus and tensile strength of graphene–epoxy nanocomposites have been reported and attributed

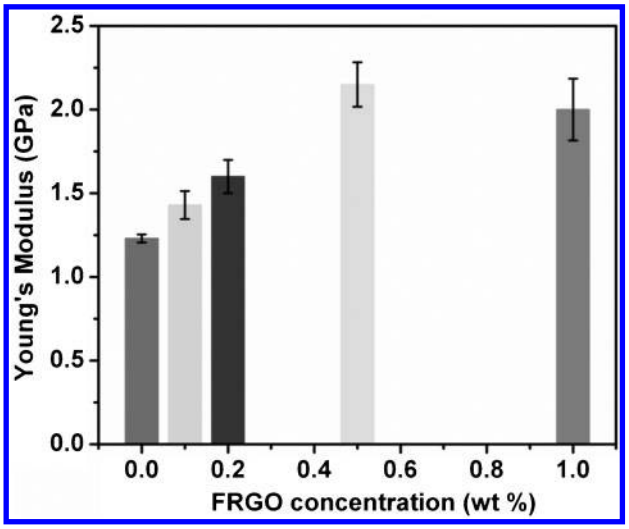

4 Young's modulus of neat epoxy and nanocomposites containing 0·1, 0·2, 0·5 and 1·0 wt-% FRGO; error bars are for three samples

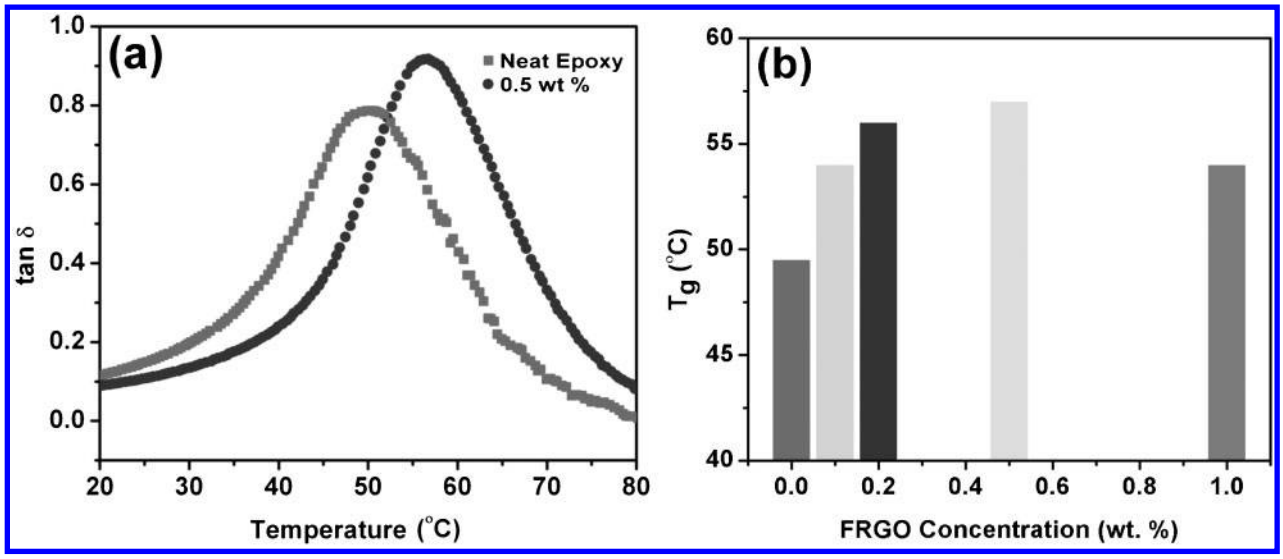

5 ***a*** **plot of tan δ versus temperature for neat epoxy and nanocomposite containing 0·5 wt-% FRGO, and** ***b*** **T_g for neat epoxy and nanocomposites containing 0·1, 0·2, 0·5 and 1·0 wt-% FRGO**

to good dispersion of graphene and strong interfacial interactions between graphene and the epoxy matrix;[11,49,50] the result is good transference of applied stress from the matrix to the FRGO.[22,49,50] With the addition of 1·0 wt-% FRGO, the Young's modulus and the tensile strength decrease by 6·7 and 13% respectively, compared to their values at 0·5 wt-%. Such a decrease has been previously reported[50–52] and attributed to the aggregation of FRGO at higher concentrations that weakens the adhesion of graphene to the matrix. It was explained that the weak adhesion reduces the stress transfer capability, which ultimately reduces the Young's modulus and tensile strength.[50–52]

As shown in Table 1, a decrease in strain at break occurs as FRGO is added. A similar observation at higher concentrations of filler has been reported and credited to the lower susceptibility of deformation of graphene compared to the matrix; thus, the filler reinforces the matrix such that it deforms less.[50,52,53] The decreased deformation indicates an increase in strength and stiffness, and is consistent with the tensile strength and the Young's modulus measurements.[53,54]

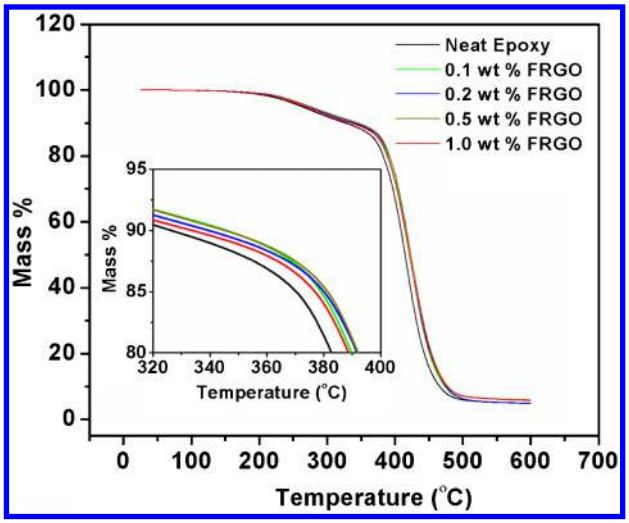

6 Thermogravimetric analysis showing mass-% versus temperature for neat epoxy and nanocomposites containing 0·1, 0·2, 0·5 and 1·0 wt-% FRGO, and ***b*** **expanded view of TGA in temperature range 320–420°C**

Dynamic mechanical analysis results

Dynamic mechanical analysis measurements provide the storage modulus E' (representing the elastic energy, that is the solid-like behaviour) and the loss modulus E'' (representing liquid-like behaviour). From these, one obtains tan $\partial = E''/E'$. In the glass transition region, E' dramatically decreases, while E'' shows a peak with a maximum. The width of the glass transition region varies, while for convenience, that region is often represented by a single number called the glass transition temperature T_g. It should be remembered that representation of a region by a single number is a large simplification.[55–58]

The onset of the drop in storage modulus as a function of temperature gives the best agreement with the peak of tan ∂. The peak in the loss modulus is often weak or absent in certain materials and not in general use.[55,57] We use the peak of tan δ for the location of T_g. This method is in common use and gives peaks with good visibility, reproducibility and minimal dependence on the analyst.[55–58] Figure 5*a* shows tan δ for neat

Table 1 Mechanical properties and glass transistion temperature T_g of neat epoxy and nanocomposites

FRGO content/wt-%	Young's modulus/GPa	Tensile strength/MPa	Strain at break/%	T_g/°C
0·0	1·23	24·1	4·39	49·5
0·1	1·43	29·1	4·22	54·0
0·2	1·60	36·1	4·03	56·0
0·5	2·14	40·6	2·92	57·0
1·0	2·00	35·2	3·48	54·0

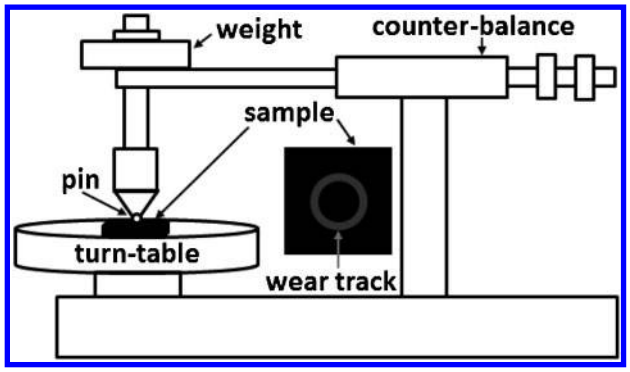

7 Schematic of pin on disc tribometer and sample

epoxy and epoxy with 0·5 wt-% FRGO. As shown in Fig. 5*b*, T_g shows a maximum at 0·5 wt-% FRGO. An increase in T_g implies an increase in interaction between the filler and matrix. The increase in T_g is consistent with previous reports using graphene platelets as fillers[23] and indicates good dispersion of FRGO in the epoxy. The decrease in T_g with further addition of FRGO may be due to the agglomeration of FRGO sheets or a reduction in cross-linking density that results in a less stiff material;[60] we have already formulated above a similar conclusion from the Young's modulus measurements.

Thermal stability

Figure 6 shows a TGA thermogram of the neat epoxy and several nanocomposites. The weight loss for the neat epoxy and nanocomposites appears to occur in two stages. In the first stage, which takes place from 200 to 360°C, both the neat epoxy and nanocomposites lose their weight by ~12%. This is attributed to a loss of adsorbed water and oligomers.[51] In the second stage, which occurs between 360 and 485°C, a significant amount of weight loss is observed and attributed to thermal decomposition of the epoxy.[28,61] The onset temperature for decomposition is ~18°C greater for nanocomposites with 0·5 wt-% FRGO than for neat epoxy. Wang *et al.* have reported a similar enhancement in the thermal stability of organosilane functionalised graphene–epoxy nanocomposites.[29]

Tribological properties in relation to microscopy results

A schematic of the tribometer we have used is shown in Fig. 7. Plots of friction versus sliding distance for the neat epoxy and several nanocomposites are shown in Fig. 8*a*. The neat epoxy exhibits an initial friction of less than or approximately equal to 0·1 during the first 1·5 m of sliding distance, as shown in the expanded view in Fig. 8*b*. After this, the friction sharply increases to 0·53. In contrast, the nanocomposites exhibit sliding distances, during which the friction is, again, less than or approximately equal to 0·1, that are more than an order of magnitude greater. As shown in Fig. 8*a* for 0·1 wt-% FRGO, the friction is less than or ~0·1 for ~44 m before increasing to 0·51. For 0·2, 0·5 and 1·0 wt-% FRGO, the friction is less than or ~0·1 for ~55, 61 and 93 m respectively before increasing to 0·43, 0·44 and 0·45 respectively.

We attribute the increase in sliding distance during which the friction is low to a transfer film from the nanocomposite to the counter surface. It is well known that transfer films reduce the friction by providing interfacial sliding between the surface and counter surface.[62] Figure 9*a* shows an optical microscopy image of the counter surface taken using a tungsten light source before any sliding. Figure 9*b* shows an image of the counter surface after sliding on the neat epoxy after a distance of 90 m; we see a clean surface with no transfer film. Figure 9*c–f* shows images of the counter surface after sliding only in the low friction regime of nanocomposites with 0·1, 0·2, 0·5 and 1·0 wt-% FRGO respectively. The images were taken after sliding a distance equal to ~50% of the distance, at which the friction sharply increases to 0·4–0·5. We observe transfer films, some of which have fringes due to interference between the incident light and the reflected light from the counter surface. Figure 10*a–d* shows images of the counter surface after sliding in the high friction regime of nanocomposites with 0·1, 0·2, 0·5 and 1·0 wt-% FRGO respectively. These images were taken after completion of the runs shown in Fig. 8*a*. Transfer films are also observed in these cases, although less coverage of the counter surface is seen.

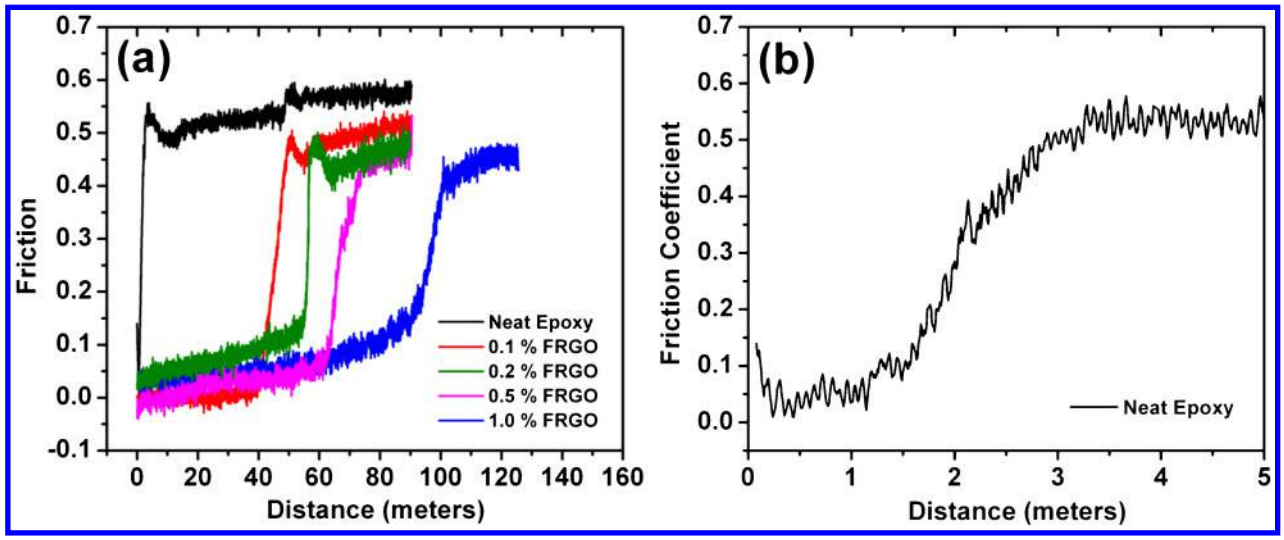

8 *a* plot of friction versus sliding distance for neat epoxy and nanocomposites containing 0·1, 0·2, 0·5 and 1·0 wt-% FRGO and *b* expanded view of friction versus sliding distance for neat epoxy

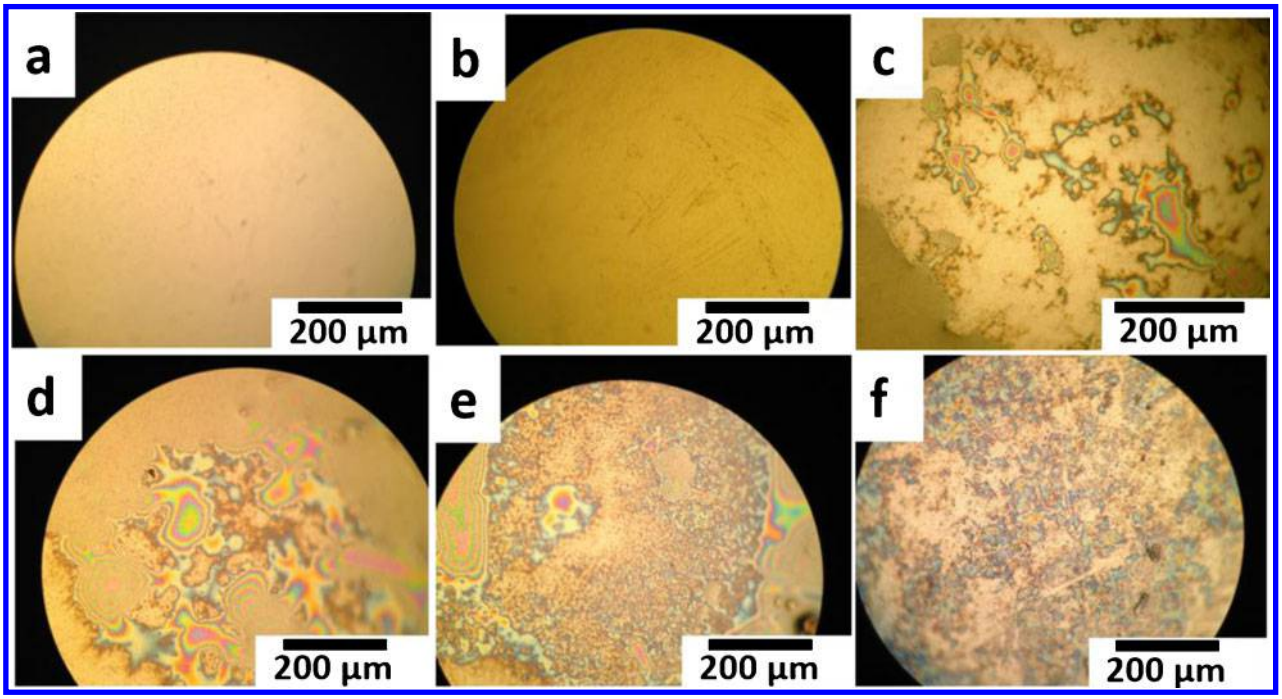

9 Optical microscopy images of countersurface: *a* clean surface and *b* surface after sliding on neat epoxy showing no transfer film and surface after sliding in low friction regime for nanocomposites containing *c* 0·1, *d* 0·2, *e* 0·5 and *f* 1·0 wt-% FRGO; transfer films are observed

The wear rates of the nanocomposites in the low and high friction regimes were calculated by measuring the depth of the wear track using a Veeco Dektak 150 profilometer. The wear behaviour of polymers can be significantly affected by fillers.[34–36,62–65] For the low friction regime, the wear track corresponding to each wt-% FRGO was measured after a sliding distance equal to ~50% of the sliding distance at which the friction sharply increases. For the high friction regime, the wear track was measured at the end of the run. The worn volume V was calculated using relation $V=\pi RA$, where R is radius of the wear track and A is the average cross-sectional area of the worn track obtained from the profilometry measurement. The wear rate W (in $mm^3\ N^{-1}\ m^{-1}$) was calculated using the relation $W=Vl/(Nx)$, where N is the normal load and x is the sliding distance. The wear rate as a function of FRGO concentration in the low and high friction regimes is

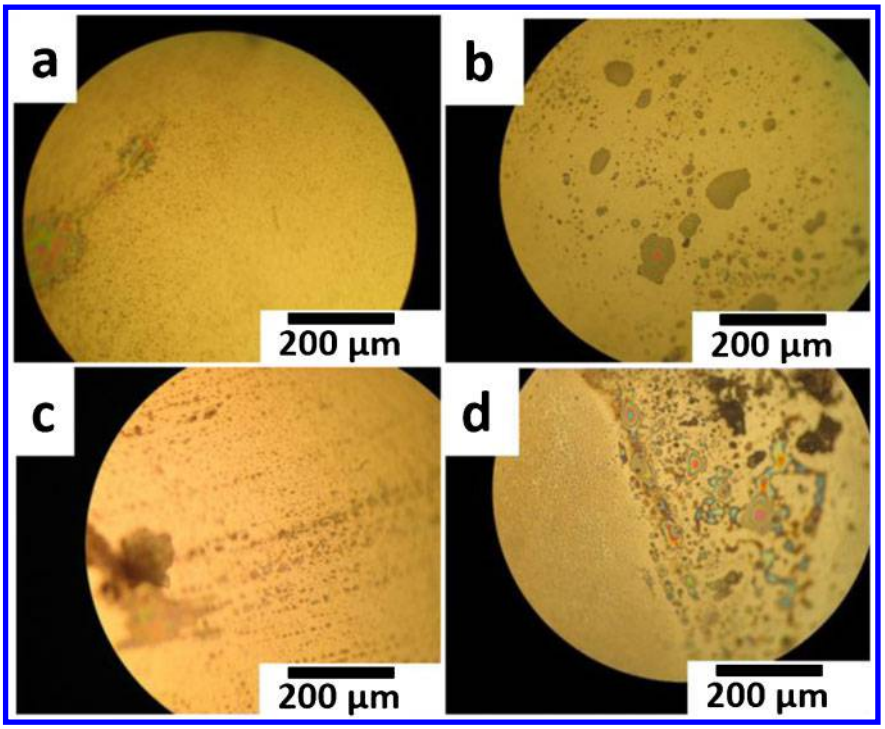

10 Optical microscopy images of countersurface after sliding in high friction regime for nanocomposite containing *a* 0·1 wt-%, *b* 0·2 wt-%, *c* 0·5 wt-% and *d* 1·0 wt-% FRGO

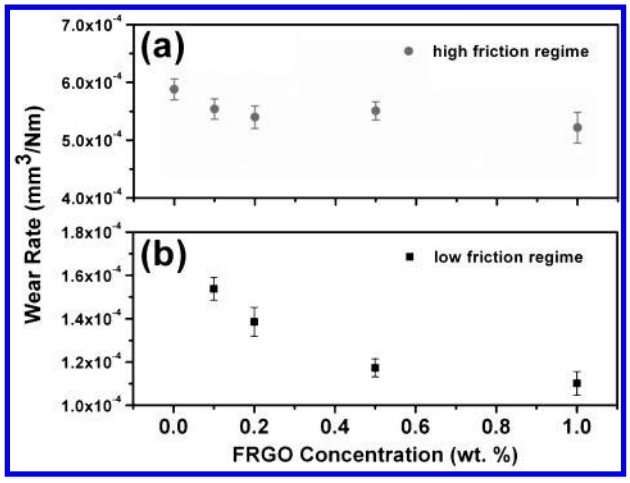

11 Wear rates of neat epoxy and nanocomposite containing 0·1, 0·2, 0·5 and 1·0 wt-% FRGO in high friction regimes and wear rates of various nanocomposites in low friction regime; error bars are for three wear tracks

shown in Fig. 11. The wear rate in the low friction regime is about five times lower than that in the high friction regime. This is attributed to the transfer film, which is also known to reduce the wear rate by isolating the surface from the counter surface and reducing frictional stresses.[37,38] In the low and high friction regimes, there is a reduction in wear rate of ~33 and 13% respectively at 1·0 wt-% FRGO.

In order to study the wear in more detail, SEM images of the wear tracks were taken. Figure 12*a* and *b* shows SEM images of the wear track of the neat epoxy near the end of the low friction regime after a sliding distance of ~3 m. Figure 12*a* shows that there are areas where the surface of the wear track has roughened. Figure 12*b* shows a magnified view of a roughened area showing the formation of wear particles. Therefore, the roughening starts near the very beginning for the neat epoxy, and this facilitates the sharp increase in friction after a very short sliding distance. Figure 12*c* and *d*, and Fig. 12*e* and *f* show SEM images of the wear tracks in the low friction regime for nanocomposites containing 0·1 and 0·5 wt-% FRGO respectively; the images were obtained after sliding distances of ~20 and 35 m respectively. For the nanocomposites, the wear tracks are significantly smoother than that of the neat epoxy even though the sliding distances are about an order of magnitude longer, and wear particles are not observed. It has been reported that a transfer film diminishes the formation of wear particles;[66] this is consistent with our observations.

Figure 13*a* and *b*, *c* and *d* and *e* and *f* show wear tracks of the neat epoxy and nanocomposites with 0·1 and 0·5 wt-% FGRO respectively in the high friction regime at the end of the run. All of the wear tracks are rough, consistent with the significantly higher friction and wear rate in this regime. The wear track of the neat epoxy is the roughest. As shown in Fig. 13*c*–*f*, when 0·1 and 0·5 wt-% FRGO are added, the wear tracks become progressively smoother. Other studies[62] have reported that the addition of fillers in an epoxy matrix forms a protective layer that reduces the wear rate. Dang *et al.* have reported similar observations with CNTs in an epoxy matrix and proposed that these fillers diminish the adhesion between the matrix and the counter surface; the digging phenomenon is thus reduced, and this results in a relatively higher wear resistance.[67]

Survey of results

The addition of FRGO in the range of 0·1–1·0 wt-% into the epoxy significantly improves the Young's modulus and tensile strength, moves up the thermal

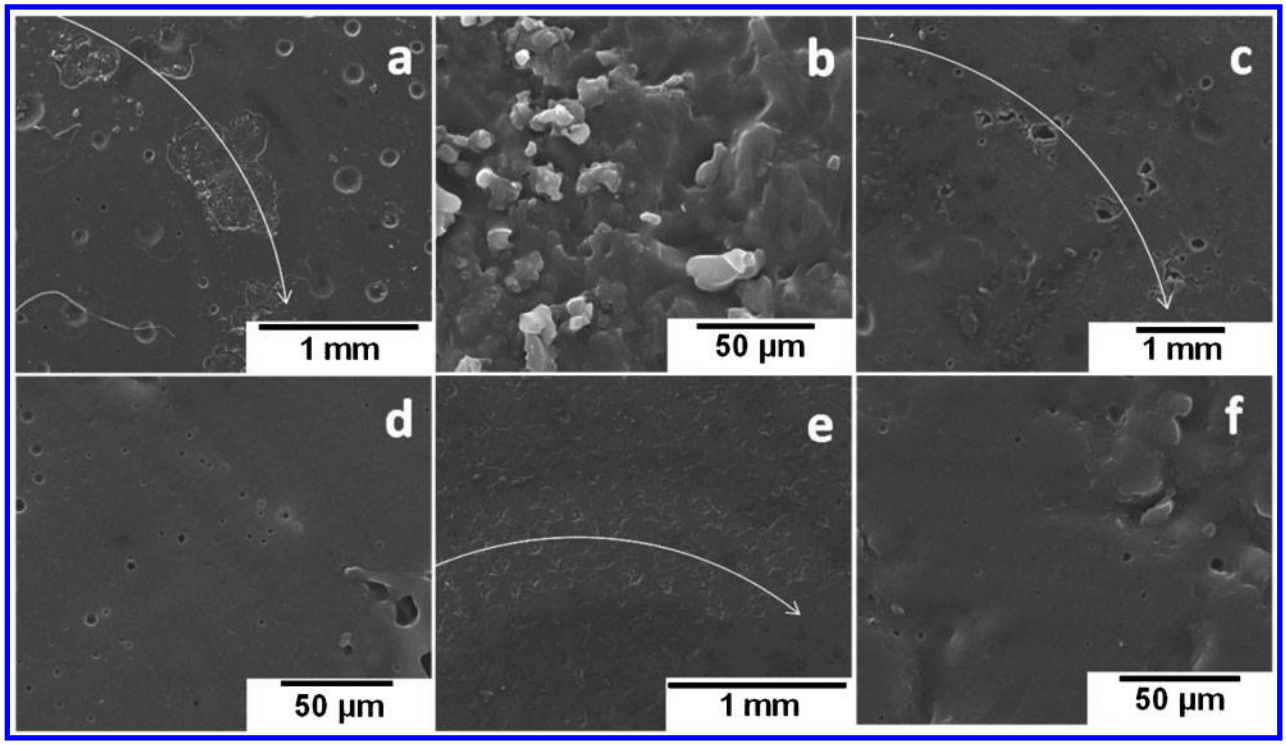

12 Images (SEM) of wear tracks in low friction regime of *a*, *b* neat epoxy, *c*, *d* nanocomposites containing 0·1 wt-% FRGO and *e*, *f* nanocomposites containing 0·5 wt-% FRGO

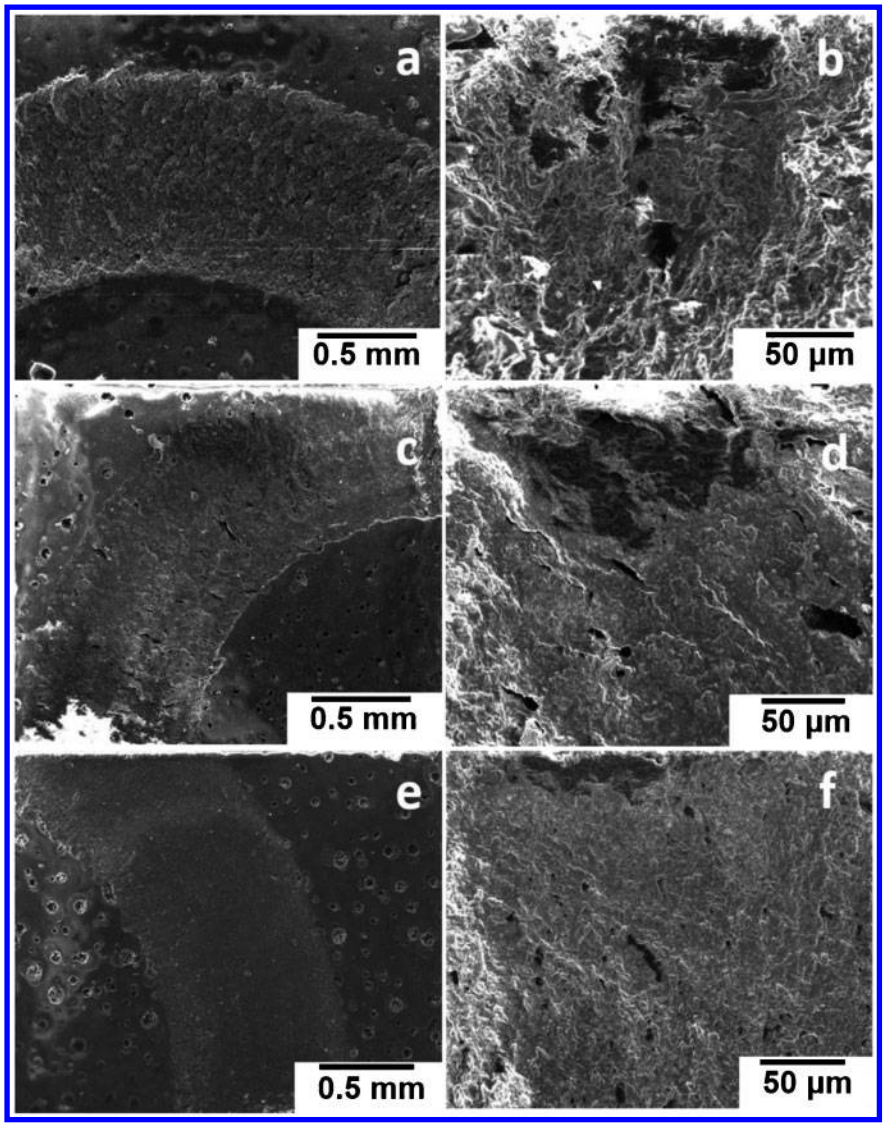

13 Images (SEM) of wear tracks in high friction regime of *a*, *b* neat epoxy, *c*,*d* nanocomposites containing 0·1 wt-% FRGO and *e*, *f* nanocomposites containing 0·5 wt-% FRGO

degradation temperature as well as the glass transition region and also lowers dynamic friction and wear. The Young's modulus and the tensile strength of the nanocomposites increase with the addition of FRGO into the epoxy and attain a maximum value at 0·5 wt-% FRGO. The upward shift in the thermal degradation temperature and T_g is highest for 0·5 wt-% FRGO. The possible reasons for these improvements could be the higher surface area of FRGO and the increased interfacial interaction between the filler and the matrix due to enhanced dispersion. The tribological studies reveal that there is improvement in the low friction sliding distance of the nanocomposites by more than an order of magnitude, after which the friction increases to 0·4–0·5. The improved frictional and wear properties are attributed to the formation of a film transfer on the counter surface, and improved mechanical interlocking arises from better adhesion of the FRGO into the epoxy matrix. While epoxies have quite a variety of applications,[32,68] the present work extends somewhat further the range of applications of this class of polymers.

Acknowledgement

We thank B. Sharma for his help in obtaining the XPS results.

References

1. K. S. Novoselov, A. K. Geim, S. V. Morozov, D. Jiang, Y. Zhang, S. V. Dubonos, I. V. Grigorieva and A. A. Firsov: 'Electric field effect in atomically thin carbon films', *Science*, 2004, **306**, 666–669.
2. A. K. Geim and K. S. Novoselov: 'The rise of graphene', *Nat. Mater.*, 2007, **6**, 183–191.
3. A. K. Geim: 'Graphene: status and prospects', *Science*, 2009, **324**, 1530–1534.
4. K. P. Loh, Q. Bao, P. K. Ang and J. Yang: 'The chemistry of graphene', *J. Mater. Chem.*, 2010, **20**, 2277–2289.
5. J. H. Jung, D. S. Cheon, F. Liu, K. B. Lee and T. S. Seo: 'A graphene oxide based immune-biosensor for pathogen detection', *Angew. Chem. Int. Ed.*, 2010, **49**, 5708–5711.
6. C. Lee, X. Wei, J. W. Kysar and J. Hone: 'Measurement of the elastic properties and intrinsic strength of monolayer graphene', *Science*, 2008, **321**, 385–388.
7. A. A. Balandin, S. Ghosh, W. Bao, I. Calizo, D. Teweldebrhan, F. Miao and C. N. Lau: 'Superior thermal conductivity of single-layer graphene', *Nano Lett.*, 2008, **8**, 902–907.

8. X. DU, I. Skachko, A. Barker and E. Y. Andrei: 'Approaching ballistic transport in suspended graphene', *Nano Lett.*, 2008, **3**, 491–495.
9. M. D. Stoller, S. Park, Y. Zhu, J. An and R. S. Ruoff: 'Graphene-based ultracapacitors', *Nano Lett.*, 2008, **8**, 3498–3502.
10. H. B. Zhang, W. Q. Zheng, Q. Yan, Y. Yang, J. Wang, Z. H. Lu, G. Y. Ji and Z. Z. Yu: 'Electrically conductive polyethylene terephthalate/graphene composite prepared by melt compounding', *Polymer*, 2010, **51**, 1191–1196.
11. T. Kuila, S. Bose, A. K. Mishra, P. Khanra, N. H. Kim and J. H. Lee: 'Effect of functionalized graphene on the physical properties of linear low density polyethylene nanocomposite', *Polym. Test.*, 2012, **31**, 31–38.
12. M. Moniruzzaman and K. I. Winey: 'Polymer nanocomposites containing carbon nanotubes', *Macromolecules*, 2006, **39**, 5194–5205.
13. J.-M. Park, D.-S. Kim, J.-R. Lee and T.-W. Kim: 'Nondestructive damage sensitivity and reinforcing effect of carbon nanotube/epoxy composites using electro-micromechanical technique', *Mater. Sci. Eng. C*, 2003, **C23**, 971–975.
14. J. Sandler, M. S. P. Shaffer, T. Prasse, W. Bauhofer, K. Schulte and A. H. Windle: 'Development of a dispersion process for carbon nanotubes in an epoxy matrix and the resulting electrical properties', *Polymer*, 1999, **40**, 5967–5971.
15. M. Russ, S. S. Rahatekar, K. Koziol, B. Farmer and H. Peng: 'Length-dependent electrical and thermal properties of carbon nanotubeloaded epoxy nanocomposites', *Compos. Sci. Technol.*, 2013, **81**, 42–47.
16. W. Brostow, M. Keselman, I. Mironi-Harpaz, M. Narkis and R. Peirce: 'Effects of carbon black on tribology of blends of poly(vinylidene fluoride) with irradiated and non-irradiated ultra-high molecular weight polyethylene', *Polymer*, 2005, **46**, 5058.
17. X. Gong, J. Liu, S. Baskaran, R. D. Voise and J. S. Young: 'Surfactant-assisted processing of carbon nanotube/polymer composites', *Chem. Mater.*, 2000, **12**, 1049–1052.
18. A. Nogales, G. Broza, Z. Roslaniec, K. Schulte, I. Sics, B. S. Hsiao, A. Sanz, M. C. Garcia Gutierrez, D. R. Rueda, C. Domingo and T. A. Ezquerra: 'Low percolation threshold in nanocomposites based on oxidized single wall carbon nanotubes and poly(butylene terephthalate)', *Macromolecules*, 2004, **37**, 7669.
19. Z. Spitalsky, D. Tasis, K. Papagelis and C. Galiotis: 'Carbon nanotube–polymer composites: chemistry, processing, mechanical and electrical properties', *Prog. Polym. Sci.*, 2010, **35**, 357–401.
20. A. Allaoui and N. El Bounia: 'How carbon nanotubes affect the cure kinetics and glass transition temperature of their epoxy composites – a review', *Express Polym. Lett.*, 2009, **3**, 588–594.
21. F. H. Gojny and K. Schulte: 'Functionalisation effect on the thermo-mechanical behavior of multi-wall carbon nanotube/epoxy-composites', *Compos. Sci. Technol.*, 2004, **64**, 2303–2308.
22. T. Ramanathan, A. A. Abdala, S. Stankovich, D. A. Dikin, M. Herrera-Alonso, R. D. Piner, D. H. Adamson, H. C. Schniepp, X. Chen, R. S. Ruoff, S. T. Nguyen, I. A. Aksay, R. K. Prud'homme and L. C. Brinson: 'Functionalized graphene sheets for polymer nanocomposites', *Nat. Nanotechnol.*, 2008, **3**, 327–331.
23. I. Zaman, T. T. Phan, H-C Kuan, Q. Meng, L. T. B. La, L. Luong, O. Youssf and J. Ma: 'Epoxy/graphene platelets nanocomposites with two level of interface strength', *Polymer*, 2011, **52**, 1603–1611.
24. R. F. Landel and L. E. Nielsen: 'Mechanical properties of polymers and composites'; 1974, New York, Marcel Dekker.
25. A. Yasmin and I. M. Danial: 'Mechanical and thermal properties of graphite platelet and epoxy composite', *Polymer*, 2004, **45**, 8211–8219.
26. M. Fang, Z. Zhang, J. Li, H. Zhang, H. Lu and Y. Yang: 'Constructing hierarchically structured interphases for strong and tough epoxy nanocomposites by amine-rich graphene surfaces', *J. Mater. Chem.*, 2010, **20**, 9635–9643.
27. S. L. Qiu, C. S. Wang, Y. T. Wang, C. G. Liu, X. Y. Chen, H. F. Xie1, Y. A. Huang and R. S. Cheng: 'Effects of graphene oxides on the cure behaviors of a tetrafunctional epoxy resin', *Express Polym. Lett.*, 2011, **9**, 809–818.
28. C. Bao, Y. Guo, L. Song, Y. Kan, X. Qian and Y. Hu: '*In situ* preparation of functionalized graphene oxide/epoxy nanocomposites with effective reinforcements', *J. Mater. Chem.*, 2011, **21**, 13290–13298.
29. X. Wang, W. Xing, P. Zhang, L. Song, H. Yang and Y. Hu: 'Covalent functionalization of graphene with organosilane and its use as a reinforcement in epoxy composites', *Compos. Sci. Technol.*, 2012, **72**, 737–743.
30. S. S. Kandanur, M. A. Rafiee, F. Yavari, M. Schrameyer, Z.-Z. Yu, T. A. Blanchet and N. Koratkar: 'Supression of wear in grapheme polymer composites', *Carbon*, 2012, **50**, 3178–3183.
31. B. Pan, S. Zhang, W. Li, J. Zhao, J. Liu, Y. Zhang and Y. Zhang: 'Tribological and mechanical investigation of MC nylon reinforced by modified grapheme oxide', *Wear*, 2012, **294–295**, 395–401.
32. B. Bilyeu, W. Brostow and K. P. Menard: 'Epoxy thermosets and their applications. I. Chemical structures and applications', *J. Mater. Educ.*, 1999, **21**, 28–286.
33. B. Bilyeu, W. Brostow and K. P. Menard: 'Epoxy thermosets and their applications. II: thermal analysis', *J. Mater. Educ.*, 2000, **22**, 107–129.
34. L. F. Giraldo, W. Brostow, E. Devaux, B. L. López and L. D. Pérez: 'Scratch and wear resistance of polyamide 6 reinforced with multiwall carbon nanotubes', *J. Nanosci. Nanotechnol.*, 2008, **8**, 1–8.
35. A. Arribas, M.-D. Bermudez, W. Brostow, F.-J. Carrion-Vilches and O. Olea-Mejia: 'Scratch resistance of a polycarbonate + organoclay nanohybrid', *Express Polym. Lett.*, 2009, **3**, 621–629.
36. W. Brostow, P. E. Cassidy, H. E. Hagg, M. Jaklewicz and P. E. Montemartini: 'Fluoropolymer addition to an epoxy: phase inversion and tribological properties', *Polymer*, 2001, **42**, 7971–7977.
37. P. J. Blau: 'Fifty years of research on wear of metals', *Tribol. Int.*, 1997, **30**, 321–331.
38. W. Brostow, V. Kovaèeviæ, D. Vrsaljko and J. Whitworth: 'Tribology of polymers and polymer-based composites', *J. Mater. Educ.*, 2010, **32**, 273–290.
39. W. S. Hummers and R. E. Offeman: 'Preparation of graphitic oxide', *J. Am. Chem. Soc.*, 1958, **80**, 1339–1339.
40. S. Stankovich, R. D. Piner, X. Chen, N. Wu, S. T. Nguyen and R. S. Ruoff: 'Stable aqueous dispersions of graphitic nanoplatelets *via* the reduction of exfoliated graphite oxide in the presence of poly(sodium 4-styrenesulfonate)', *J. Mater. Chem.*, 2006, **16**, 155–158.
41. T. Kuilla, S. Bhadra, D. Yao, N. H. Kim, S. Bose and J. H. Lee: 'Recent advances in graphene based polymer nanocomposites', *Prog. Polym. Sci.*, 2010, **35**, 1350–1375.
42. Y. Geng, S. J. Wang and J. K. Kim: 'Preparation of graphite nanoplatelets and graphene sheets', *J. Colloid Interface Sci.*, 2009, **336**, 592–598.
43. T. Wei, G. Luo, Z. Fan, C. Zheng, J. Yan, C. Yao, W. Li and C. Zhang: 'Preparation of graphene nanosheet/polymer composites using in situ reduction-extractive dispersion', *Carbon*, 2009, **47**, 2290–2299.
44. A. B. Bourlinos, D. Gournis, D. Petridis, T. Szabo, A. Szeri and I. Dekany: 'Graphite oxide: chemical reduction to graphite and surface modification with primary aliphatic amines and amino acids', *Langmuir*, 2003, **19**, 6050–6055.
45. C. Zhu, S. Guo, Y. Fang and S. Dong: 'Reducing sugar: new functional molecules for the green synthesis of graphene nanosheets', *ACS Nano*, 2010, **4**, 2429–2437.
46. S. Stankovich, D. A. Dikin, R. D. Piner, K. A. Kohlhaas, A. Kleinhammes, Y. Jia, Y. Wu, S. T. Nguyen and R. S. Ruoff: 'Synthesis of graphene-based nanosheets via chemical reduction of exfoliated graphite oxide', *Carbon*, 2007, **45**, 1558–1565.
47. K. N. Kudin, B. Ozbas, H. C. Schniepp, R. K. Prud'homme, I. A. Aksay and R. Car: 'Raman spectra of graphite oxide and functionalized graphene sheets', *Nano Lett.*, 2008, **8**, 36–41.
48. W. Li, X.-Z. Tang, H.-B. Zhang, Z.-G. Jiang, Z.-Z. Yu, X.-S. Du and Y-W. Mai: 'Simultaneous surface functionalization and reduction of graphene oxide with octadecylamine for electrically conductive polystyrene composites', *Carbon*, 2011, **49**, 4724–4730.
49. M. A. Rafiee, J. Rafiee, Z. Wang, H. Song, Z.-Z. Yu and N. Koratkar: 'Enhanced mechanical properties of nanocomposites at low graphene content', *ACS Nano*, 2009, **3**, 3884–3890.
50. M. A. Rafiee, W. Lu, A. V. Thomas, A. Zandiatashbar, J. Rafiee, J. M. Tour, and N. A. Koratkar: 'Graphene nanoribbon composites', *ACS Nano*, 2010, **4**, 7415–7420.
51. S. Kim, I. Do and L. T. Drzal: 'Multifunctional xGnP/LLDPE nanocomposites prepared by solution compounding using various screw rotating systems', *Macromol. Mater. Eng.*, 2009, **294**, 196–205.
52. T. Kuila, P. Khanra, A. K. Mishra, N. H. Kim and J. H. Lee: 'Functionalized-graphene/ethylene vinyl acetate co-polymer composites for improved mechanical and thermal properties', *Polym. Test.*, 2012, **31**, 282–289.
53. A. Romisuhani, H. Salmah and A. Akmal: 'Tensile properties of low density polypropylene (LDPE)/palm kernel shell (PKS)

bio-composites: the effect of acrylic acid (AA)', *Mater. Sci. Eng.*, 2010, **11**, 1–7.
54. K. Oksman and C. Clemons: 'Mechanical properties of polypropylene-wood and morphology of impact modified floor composites', *J. Appl. Polym. Sci.*, 1998, **67**, 1503–1513.
55. K. P. Menard: 'Dynamic mechanical analysis: a practical introduction', 2nd edn, 103; 2008, Boca Raton, FL, CRC Press.
56. R. J. Seyler: 'Assignment of the glass transition'; 1994, Baltimore, MD, American Society for Testing and Materials.
57. I. M. Kalogeras and H. E. Hagg Lobland: 'The nature of the glassy state: structure and transitions', *J. Mater. Educ.*, 2012, **34**, 69–94.
58. J. Reiger: 'The glass transition temperature T_g of polymers—comparison of the values from differential thermal analysis (DTA, DSC) and dynamic mechanical measurements (torsion pendulum)', *Polym. Test.*, 2001, **20**, 199–204.
59. H. F. Mark, N. M. Bikales, C. G. Overberger and G. Menges: 'Encyclopedia of Polymer Science and engineering', 2nd edn, 7; 1987, New York, John Wiley & Sons.
60. H. Kim, A. Abdala and C. Macosko: 'Graphene/polymer nanocomposites in graphite, graphene, and their polymer nanocomposites'; 2012, Boca Raton, FL, CRC Press.
61. B. Bilyeu, W. Brostow and K. P. Menard: 'Epoxy thermosets and their applications. III: kinetic equations and models', *J. Mater. Educ.*, 2001, **23**, 189.
62. W. Brostow, W. Chonkaew, K. P. Menard and T. W. Scharf: 'Modification of an epoxy resin with a fluoroepoxy oligomer for improved mechanical and tribological properties', *Mater. Sci. Eng. A*, 2009, **A507**, 241–251.
63. A. de la Isla, W. Brostow, B. Bujard, M. Estevez, R. Rodriguez, S. Vargas and V. M. Castaño: 'Nanohybrid scratch resistant coatings for teeth and bone viscoelasticity manifested in tribology', *Mater. Res. Innov.*, 2003, **7**, 110–114.
64. M. Estevez, S. Vargas, A. de la Isla, W. Brostow, V. M. Castaño and J. R. Rodriguez: 'Anovel dental material with high scratch resistance', *Mater. Res. Innov.*, 2005, **9**, 80–81.
65. B. Bilyeu, W. Brostow, L. Chudej, M. Estevez, H. E. Hagg Lobland, J. R. Rodriguez and S. Vargas: 'Scratch resistance of different silica filled resins for obturation materials', *Mater. Res. Innov.*, 2007, **11**, 181–184.
66. M. C. Romanes, N. A. D'Souza, D. Coutinho, K. J. Balkus Jr. and T. W. Scharf: 'Surface and subsurface characterization of epoxy-mesoporous silica composites to clarify tribological properties', *Wear*, 2008, **265**, 88–96.
67. B. Dong, Z. Yang, Y. Huang and H.-L. Li: 'Study on tribological properties of multi-walled carbon nanotubes/epoxy resin nanocomposites', *Tribol. Lett.*, 2005, **20**, 251–254.
68. W. Brostow, S. H. Goodman and J. Wahrmund: 'Epoxies', in 'Handbook of thermoset plastics', (ed. H. Dodiuk and S. H. Goodman), Chap. 8, 3rd edn; 2014, Oxford, Elsevier.